



Double-nano silica xerogel contributes to establish nifedipine delivery system with superior delivery effect

Ping Zhang, Qiankun Jiang, Yue Zheng, Jing Li*

School of Pharmacy, Shenyang Medical College, Shenyang, China

ARTICLE INFO

Keywords:

Double-nano silica xerogel
Micelles
Poorly water soluble drug
Drug delivery

ABSTRACT

To further explore the wonder of nano technology in drug delivery system, the combination of micelles and mesoporous silica was conducted for delivering poorly water soluble nifedipine (NFP). Double-nano silica xerogel (DN-SX) with both micelles and nanopores was prepared and silica xerogel with only nanopores (SN-SX) was made for comparison. Characteristics of DN-SX and SN-SX, including morphology, porous structure and crystalline state were investigated and pharmaceutical performances of drug loaded carriers were studied. The micelles in DN-SX contributed to achieve larger mesopores and enhanced NFP dissolution better than SN-SX. How responses of drug release amount and reduced drug release amount reacted as changing each influencing factor was elucidated by Box–Behnken experimental design. With the DN-SX obtained by optimization, in vivo pharmacokinetic study result demonstrated that the relative bioavailability of NFP loaded DN-SX and NFP loaded SN-SX were 216.84% and 161.14%, respectively. Therefore, the optimized DN-SX with double-nano structure was of great value for designing poorly water soluble drug delivery system.

1. Introduction

It is widely known that nanotechnology is a multidisciplinary field to design materials or devices with dimensions in the nanometer range. In the past few decades since its emergence, nanotechnology provides a large number of strategies to prevent, diagnose, treat diseases, and repair tissues by using nanomaterials with unique optical, thermal, magnetic or redox properties. Also, nanotechnology has brought huge benefits for pharmaceutical field by introducing nanomaterials into various kinds of drug delivery systems [1,2]. In the current stage, nanotechnology can be realized by using organic and inorganic nanomaterials. Organic materials with good biocompatibility and biodegradability, such as nanoparticles, micelles, dendrimers, liposomes, etc, have low level of stability and functionality. On the contrary, inorganic materials with high stability and functionality present relative low biocompatibility and biodegradability, which rouse their safety concern. The widely studied inorganic nanomaterials mainly include nanoporous silica, carbon and metal oxide-based nanoparticles [2–4]. Inorganic materials with porous structure in the nano range can be also considered as nanomaterials. Among these nanomaterials, micelles are formed by the hydrophobic interaction among the lipophilic molecules and the repulsive forces between the hydrophilic groups. There are two kinds of

micelles, which are unimolecular and multi-molecular micelles [5]. Micelle can be used as an effective tool for loading poorly water soluble drug with ability to increase drug solubility, dissolution and even transmembrane permeability [6–8].

Among the large profound of nanomaterials, silica materials with nanopores turn out to be an effect tool to establish drug delivery systems owing to its nano pores, and the typical example is mesoporous silica materials. Mesoporous silica materials display wide biomedical applications owing to their high chemical stability, large surface area and tunable pore diameters and volumes. The advantage of applying mesoporous silica is that it can allow the incorporation of large amounts of drug and protect the loaded drug from deactivation and degradation [9–11]. Silica materials with nanopores can be widely employed as multifunctional platforms to construct drug delivery systems. The carrier incorporates drugs by (1) electrostatic adsorption or hydrophobic interactions; (2) covalently grafting drugs on the surface/inside porous channels via chemical bonding; (3) doping drugs during the synthesized process, which is called one-pot method [12]. Drug delivery systems established by silica materials with nanopores can exert functions to control drug release, improve drug dissolution or enhance drug effect, etc [13–19]. With the increasing number of innovative new drugs to be explored, almost 70% of new drug candidates have low aqueous

* Corresponding author. Address: No. 146 Huanghe North Street, Shenyang, Liaoning Province, China.

E-mail address: dddefghijklmn@163.com (J. Li).

<https://doi.org/10.1016/j.micromeso.2019.109996>

Received 24 November 2019; Received in revised form 26 December 2019; Accepted 29 December 2019

Available online 2 January 2020

1387-1811/© 2020 Elsevier Inc. All rights reserved.

solubility, which significantly limits their application. Towards this, silica materials with nanopores turn out to be an effective strategy to improve drug dissolution and bioavailability of poorly water soluble drugs. For example, indometacin [20], simvastatin [14] and famotidine [21] have been used to load into silica materials with nanopores and performed superior effects.

To further explore the wonder of nano technology in drug delivery system, the combination of micelles and mesoporous silica was tried for delivering poorly water soluble drug. Since micelles and nanopores both presented in the silica xerogel, it belonged to double-nano silica xerogel and named it as DN-SX. For comparison, the silica xerogel with only nanopores was prepared and called SN-SX. The model drug chose a poorly water soluble drug nifedipine (NFP). It is used for prevention and treatment of coronary heart disease angina pectoris, especially variant angina pectoris and coronary artery spasm caused by angina pectoris. It has no adverse effect on respiratory function, thus rendering it suitability for patients with obstructive respiratory disease. Furthermore, it is also applicable to various types of hypertension and has good curative effect on refractory and severe hypertension [22]. The capacity of DN-SX in managing drug dissolution was mainly studied using Box-Behnken design and the optimized DN-SX performed the best ability in improving drug dissolution and maintaining high level of drug release amount.

2. Materials and methods

2.1. Materials

Tetramethoxysilane (TMOS) was purchased from Aladdin (Shanghai, China), and all other chemical reagents were bought from China. Deionized water was prepared by ion exchange.

2.2. One-pot preparation of DN-SX and SN-SX

1 wt% polyethylenimine (PEI) solution and 50 mg/mL hydroxy propyl methyl cellulose (HPMC) E5 solution were prepared using deionized water before the synthesis of DN-SX and SN-SX. 0.1 mL PEI solution was mixed with 0.1 mL HPMC E5 solution and the above mixture was blended with 0.5 mL TMOS. The colloidal system was left at ambient conditions statically until the formation of wet gel. Finally, wet gel was dried at vacuum drying oven to remove volatile solvent to finally get DN-SX. For highlighting the advantage of double-nano design in DN-SX, SN-SX was prepared using the similar working process except that no HPMC E5 solution was added into the reactive system. To demonstrate the micelles of HPMC E5 in the reaction system of DN-SX, particle size of HPMC E5 solution was measured by Malvern Zetasizer (Nano ZS, Malvern Co., USA), and particle size of deionized water solution was also tested for SN-SX. The measurement was performed in triplicate.

2.3. Characterization

SEM images of DN-SX and SN-SX were characterized using SURA 35 field emission scanning electron microscope (ZEISS, Germany). Samples were pasted onto metal stubs and sputtered with gold under vacuum.

The surface area and pore volume of DN-SX and SN-SX were studied by determining the nitrogen adsorption/desorption using V-Sorb 2800P (app-one, China). The specific surface area was evaluated according to nitrogen adsorption data. Pore size distributions were obtained from adsorption branches of isotherms. The total pore volume was determined from the amount adsorbed at a relative pressure of 0.99.

2.4. Drug loading procedure and property

NFP was loaded into carriers using one-pot method. 0.1 mL PEI solution was mixed with 0.1 mL HPMC E5 solution and the above mixture was blended with drug solution then 0.5 mL TMOS. The colloidal system

Table 1

Variables in Box–Behnken experimental design of DN-SX.

Factor	Level	
	−1	+1
X ₁ Pore diameter (nm)	2.8	4.5
X ₂ HPMC E5 solution (mL)	0.05	0.2
X ₃ TMOS (mL)	0.02	1.0
Response	Constraints	
Y ₁ Drug release amount (%)	Maximize	
Y ₂ Reduced release amount (%)	Minimize	

was left at ambient conditions statically until the formation of wet gel. Finally, wet gel was dried at vacuum drying oven to remove volatile solvent to finally get NFP loaded DN-SX. Similarly, NFP loaded SN-SX was prepared using the same working process except that no HPMC E5 solution was added in the system.

Drug loading amount was calculated by subtracting the loaded drug using absolute ethyl alcohol from carrier and analyzed drug amount using UV-6100S (Shanghai, China) at 238 nm. The standard curve for calculating drug concentration was $A = 0.0305C - 0.0375$ ($R^2 = 0.9998$). The measurement was performed in triplicate.

$$\text{Drug loading capacity (\%)} = (W_{\text{drug in carrier}} / W_{\text{drug loaded carrier}}) \times 100$$

The crystalline state of SN-SX, DN-SX, NFP, NFP loaded SN-SX and NFP loaded DN-SX was evaluated using differential scanning calorimeter (DSC, Q1000, TA Instrument, USA). Samples were placed in pierced aluminum pans and heated at a scanning rate of 10 °C/min under nitrogen protection.

Infrared spectroscopy (IR, Spectrum 1000, PerkinElmer, USA) spectra of samples were obtained over the spectral region 400 to 4000 cm^{-1} . Samples were prepared by gently and respectively grounding samples with KBr.

2.5. In vitro drug dissolution and wetting property

In vitro dissolution experiment was carried out using USP paddle method (100 rpm, 37 °C) with RC806D dissolution tester (Shanghai, China). Samples were exposed to simulated gastric fluid (pH 1.0 hydrochloric acid). At predetermined time intervals, 5 mL dissolution medium was withdrawn from the release medium and the same amount of new dissolution medium was added. The withdrawn dissolution medium was administered through 0.45 μm microporous membrane then analyzed using UV-6100S (Shanghai, China) at the wavelength of 238 nm. The measurement was performed in triplicate.

The contact angle was measured using contact angle meter model JCY series (Shanghai, China) with automatic model. The same amount of sample powder was compressed using a steel punch and die assembly under the same pressure. Dissolution medium (20 μL) was dropped onto the surface of table and images were recorded until the medium completely wetted into the sample. The contact angle of each image was obtained using the software provided by contact angle meter model JCY series. The measurement was conducted in triplicate.

2.6. Regulation drug release

A three-level two-factorial Box–Behnken experimental design (Design Expert, Version 8.0.6, Stat-Ease Inc., Minneapolis, MN) was used [23] to evaluate the effects of pore diameter, HPMC E5 solution and TMOS on drug release behavior. Box-Behnken statistical design has been used to analyze how important parameters affect the independent variables. It is considered as an independent, rotatable or nearly rotatable, quadratic design. Many experimental runs and time are saved using this experiment design to screen expected working conditions. The factors chosen and settings of factor levels were presented in Table 1, and each experiment was shown in Table 2. The selected responses were drug

release amount and reduced drug release amount. Drug release amount was one important parameter to determine the highest drug release level, and reduced drug release amount reflected the ability of

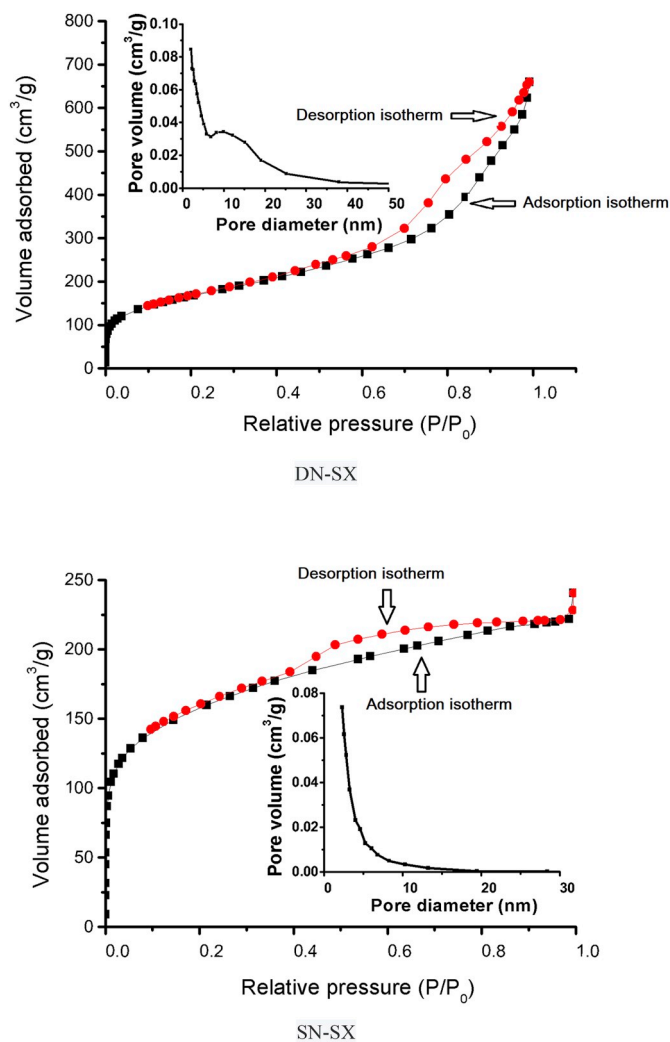


Fig. 2. Nitrogen adsorption-desorption isotherm and pore size distribution curve of DN-SX and SN-SX.

3. Results and discussions

3.1. Characteristics

After measuring the particle size of HPMC E5 solution for DN-SX system, it was clear that micelles were formed since the mean particle size turned out to be 25.9 ± 1.8 nm. On the contrary, the mean particle size of deionized water solution for SN-SX system was 0.4 ± 0.1 nm, showing that no micelles were in the reaction solution of SN-SX. SEM images in Fig. 1 showed that both DN-SX and SN-SX were quite small nanoparticles aggregated intensively due to xerogel state. It should be noted that DN-SX nanoparticles gathered and shaped like big spherical particles while not for SN-SX nanoparticles, demonstrating that the micelles in DN-SX were able to induce the silica polycondensation around and formed big particles. Porous structure of DN-SX and SN-SX was presented in Fig. 2. It was obvious that there were hysteresis loops in the relative pressure of 0.5–1.0 for DN-SX and 0.4–0.8 for SN-SX, showing their mesopores within the silica frame. The specific surface area and pore volume of DN-SX were $598.7 \text{ cm}^2/\text{g}$ and $0.95 \text{ cm}^3/\text{g}$, which was larger than SN-SX ($551.3 \text{ cm}^2/\text{g}$ and $0.20 \text{ cm}^3/\text{g}$). The pore diameter of DN-SX divided into two groups, one located around 10 nm and the other group was smaller than 3 nm. Compared to the porous distribution of DN-SX, SN-SX only displayed mesopores of smaller than 3 nm, demonstrating that the micelles in DN-SX contributed to obtain

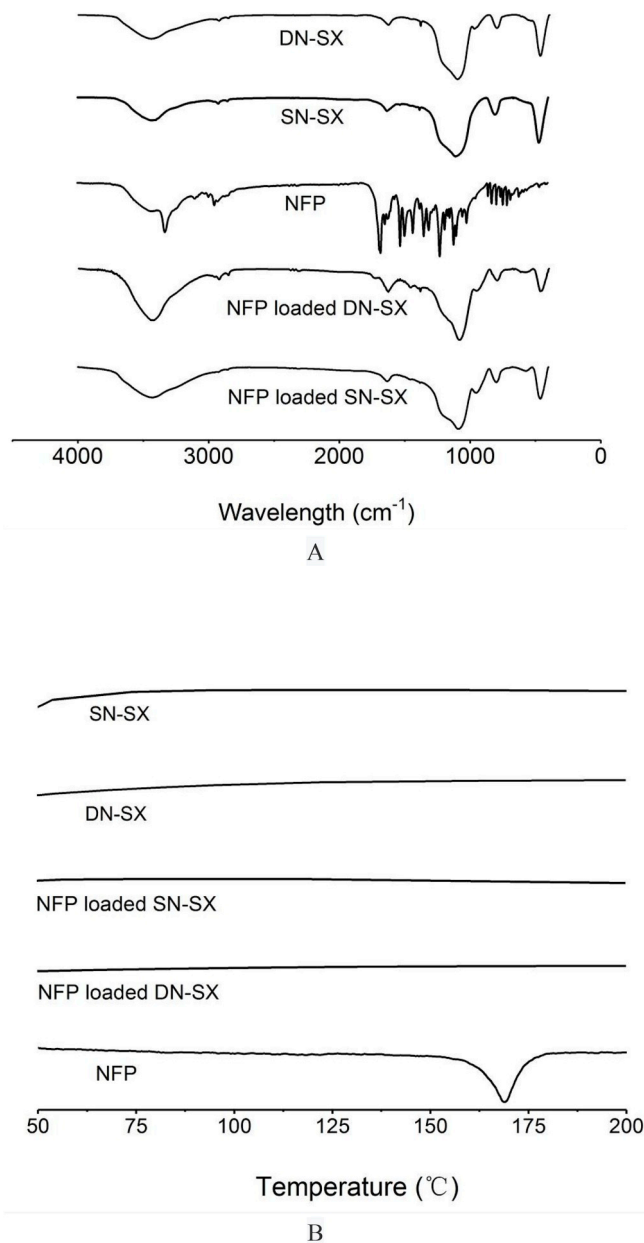


Fig. 3. A, IR spectra of DN-SX, SN-SX, NFP, NFP loaded of DN-SX and NFP loaded SN-SX; B, DSC curves of SN-SX, DN-SX, NFP loaded SN-SX, NFP loaded of DN-SX and NFP.

larger mesopores and resulted in higher surface area and significant larger pore volume. Moreover, the large specific surface area and pore volume rendered the two carriers capacity to be carriers for loading small molecular drugs.

3.2. IR and DSC

IR spectra of DN-SX and SN-SX displayed their characteristic peaks of silica, including Si–O–Si bending vibration located around 464.8 cm^{-1} , Si–O–Si symmetric stretching vibration at about 798.2 cm^{-1} , Si–O–Si antisymmetric stretching vibration at around 1091.6 cm^{-1} , H–O–H bending vibration located around 1633.0 cm^{-1} and O–H of Si–OH antisymmetric stretching vibration at about 3434.5 cm^{-1} . The result demonstrated that only silica peaks can be tested out in their IR analysis and there were no differences between DN-SX and SN-SX. IR spectrum of NFP (Fig. 3A) showed its characteristic peaks at a number of

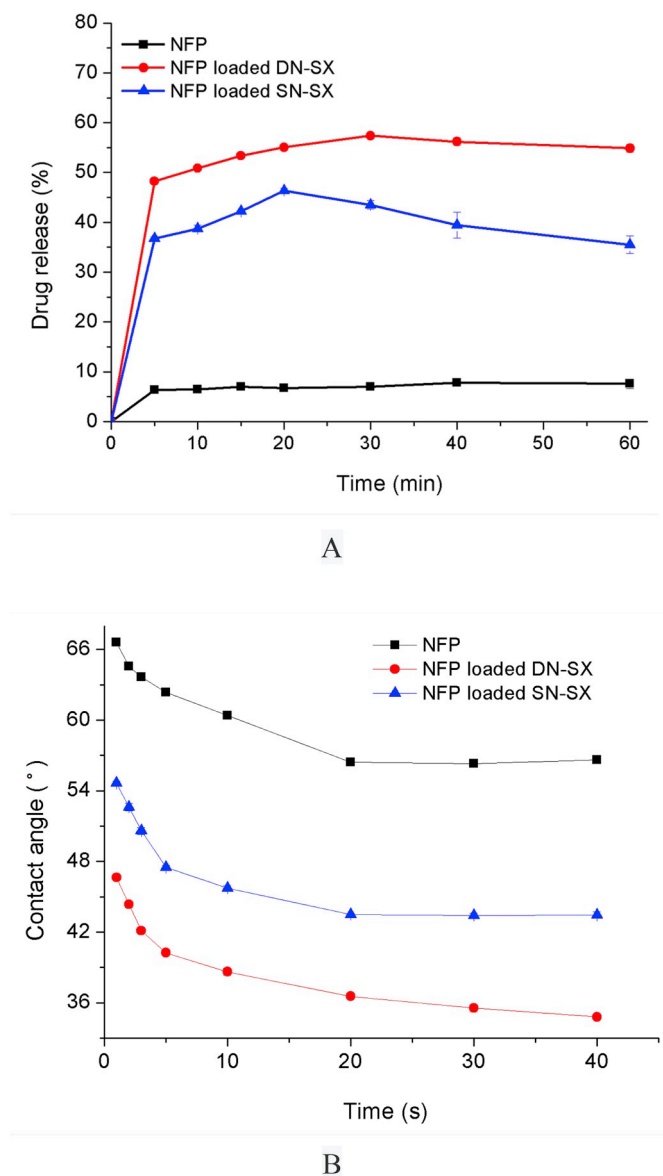


Fig. 4. A, Drug dissolution of NFP, NFP loaded of DN-SX and NFP loaded SN-SX; B, Dynamic contact angle of NFP, NFP loaded of DN-SX and NFP loaded SN-SX.

wavelengths, including 3330.3 cm^{-1} (N–H stretching vibration), 2952.1 cm^{-1} (C–H stretching vibration), 1679.3 cm^{-1} (C=O stretching vibration), 1647.1 cm^{-1} (C=C stretching vibration), 1529.7 cm^{-1} (N=O stretching vibration), 1496.4 cm^{-1} and 1432.7 cm^{-1} (Benzene ring skeleton vibration), 1349.3 cm^{-1} (C–N stretching vibration), 1310.9 cm^{-1} and 1226.9 cm^{-1} (N–O stretching vibration), 1120.9 cm^{-1} , 1101.2 cm^{-1} and 1021.7 cm^{-1} (C–O stretching vibration). After being loaded into the two carriers, almost all drug peaks had been covered and only presented characteristic peaks of silica, including Si–O–Si bending vibration at around 462.3 cm^{-1} , Si–O–Si symmetric stretching vibration at around 799.1 cm^{-1} , Si–O–Si antisymmetric stretching vibration at around 1090.8 cm^{-1} , H–O–H bending vibration at around 1631.4 cm^{-1} and O–H of Si–OH antisymmetric stretching vibration at around 3433.0 cm^{-1} , demonstrating that NFP was well loaded into the pores of carriers. As shown in Fig. 3B, DSC curves of SN-SX and DN-SX were lines without any peaks, demonstrating their amorphous state. DSC profile of NFP clearly showed drug melting peak, confirming the crystalline state of NFP. However, after being loaded into DN-SX and SN-SX, drug melting peak can not be observed because crystal drug converted to amorphous

phase in the mesopores of the two carriers.

3.3. NFP release and wetting property

After calculating, the drug loading amount of NFP loaded DN-SX was $8.2 \pm 1.3\%$ and NFP loaded SN-SX turned out to be $7.9 \pm 0.6\%$, demonstrating that no obvious difference of drug loading amount for the two drug loading systems. As for NFP release, both SN-SX and DN-SX significantly improved drug dissolution by almost 9 times and 11 times compared to NFP (Fig. 4A). The enhanced NFP release mainly contributed to their ability in converting crystal NFP to amorphous NFP evidenced by DSC analysis. The loaded drug was limited within the mesopores and therefore avoiding the growth of crystal drug. Compared with the crystal drug, the amorphous drug can reduce the lattice energy, resulting in enhanced dissolution. In addition, the large hydrophilic surface area of carriers facilitated the wetting and dispersion of the loaded drug, which was also favorable for achieving fast drug release. It showed that the drug release of NFP loaded DN-SX (almost 57%) was higher than NFP loaded SN-SX (almost 35%), demonstrating that the second nano in DN-SX, which was the micelles, exerted extra function in improving drug dissolution owing to its ability to increase drug solubility [13,18,29]. More importantly, the micelles also remained high level of released amorphous drug and the reduced drug release was only 2.5%, while the reduced drug release of NFP loaded SN-SX reached to 10.9%. The enhanced drug dissolution can be also elucidated by the wetting property result (Fig. 4B). Since the loaded NFP was amorphous state, the wetting of NFP loaded SN-SX and NFP loaded DN-SX turned out to be obvious superior than NFP, which confirmed the advantage of applying SN-SX and DN-SX in improving NFP dissolution. The contact angle of NFP loaded DN-SX was lower than NFP loaded SN-SX, showing that the micelles in DN-SX contributed the achievement of better wetting property and further superior drug dissolution. Moreover, the contact angle in the range of 20 s–40 s possibly reflected the ability of carrier in remaining amorphous drug state. In this time period, the contact angle of NFP loaded SN-SX almost did not change and so did the contact angle of NFP. However, the contact angle of NFP loaded DN-SX still changed lower through with time, demonstrating that the wetted NFP in DN-SX can remain its amorphous state without interfering the wetting process in 20 s–40 s. While NFP loaded SN-SX as well as NFP with almost no change of wetting in this time phase failed to perform this ability due to the lack of micelles. The above drug release and wetting property results confirmed the superior drug dissolution of NFP loaded DN-SX than both NFP and NFP loaded SN-SX.

3.4. Box–Behnken experimental design

3.4.1. Model fitting

After conducting Box–Behnken design based on experimental data, fit summary of each response was initially obtained. Among linear, 2FI and Quadratic models, drug release amount fitted to 2FI model and reduced release amount was in accordance with linear model. The calculated equations were shown below:

$$Y_1 = +40.13 + 4.46X_1 + 14.21X_2 + 6.47X_3 - 5.25X_1X_2 - 2.34X_1X_3 + 20.05X_2X_3 \quad (1)$$

$$Y_2 = +0.62 + 1.54X_1 - 39.09X_2 + 24.64X_3 + 9.16X_1X_2 - 8.76X_1X_3 + 19.73X_2X_3 \quad (2)$$

In the reaction process, pore diameter was in the range of 2.8–4.5 nm, HPMC E5 solution was in the range of 0.05–0.2 mL and TMOS solution was chosen among 0.02–1.0 mL. The application range of HPMC E5 and TMOS was determined to make sure the carrier can be formed since the synthesis of silica materials accomplished at a certain level of working conditions. The influences of each factor on the two responses from the chosen levels were displayed in Fig. 5. It was obvious that drug

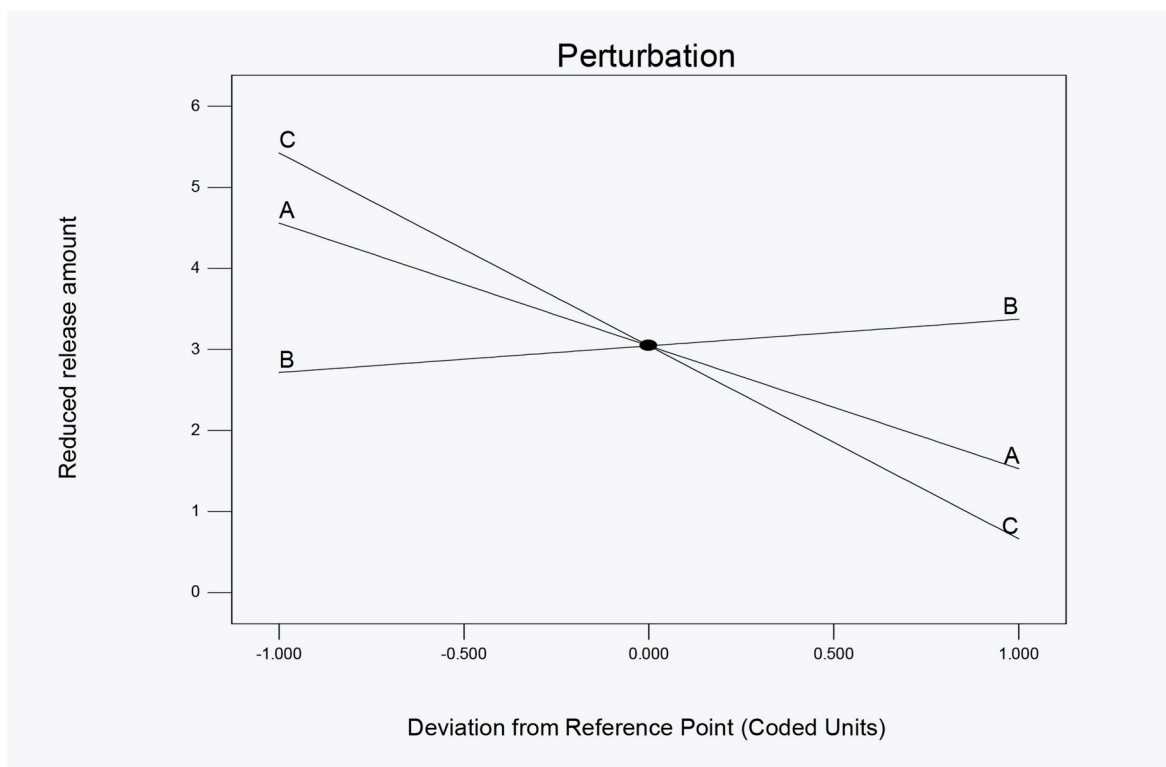
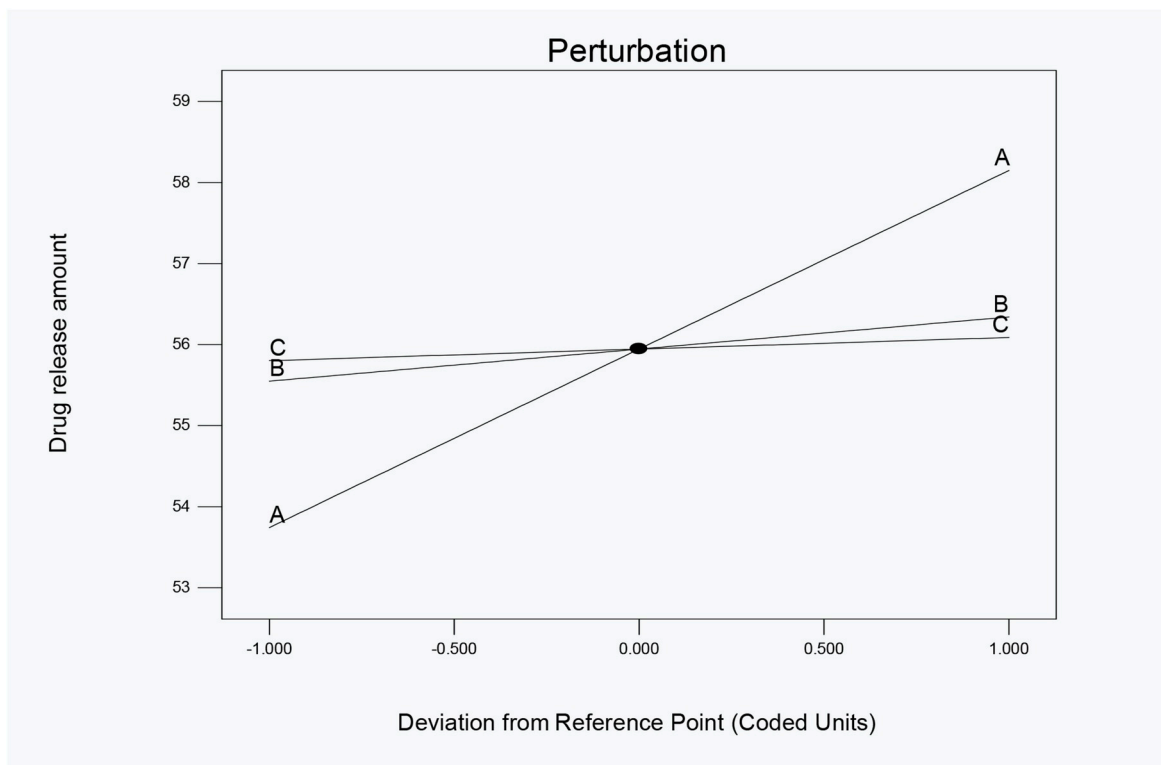


Fig. 5. Perturbation plots effects of X_1 (A), X_2 (B) and X_3 (C) on responses Y_1 and Y_2 .

release amount was positively related with the three factors and HPMC E5 was the strongest parameter in determining drug release amount, demonstrating that the larger pore diameter and the higher drug dissolution. As for reduced drug release amount, only HPMC E5 was positively related with it, indicating that the more micelles in the

system, the better ability to remain high level of released drug with amorphous state. The specific effects of parameters on responses were shown in the following contour plots and response surface analysis.

Since pore diameter was the nature of carrier, it was mainly determined by the amount of HPMC E5 and TMOS. Generally, the higher

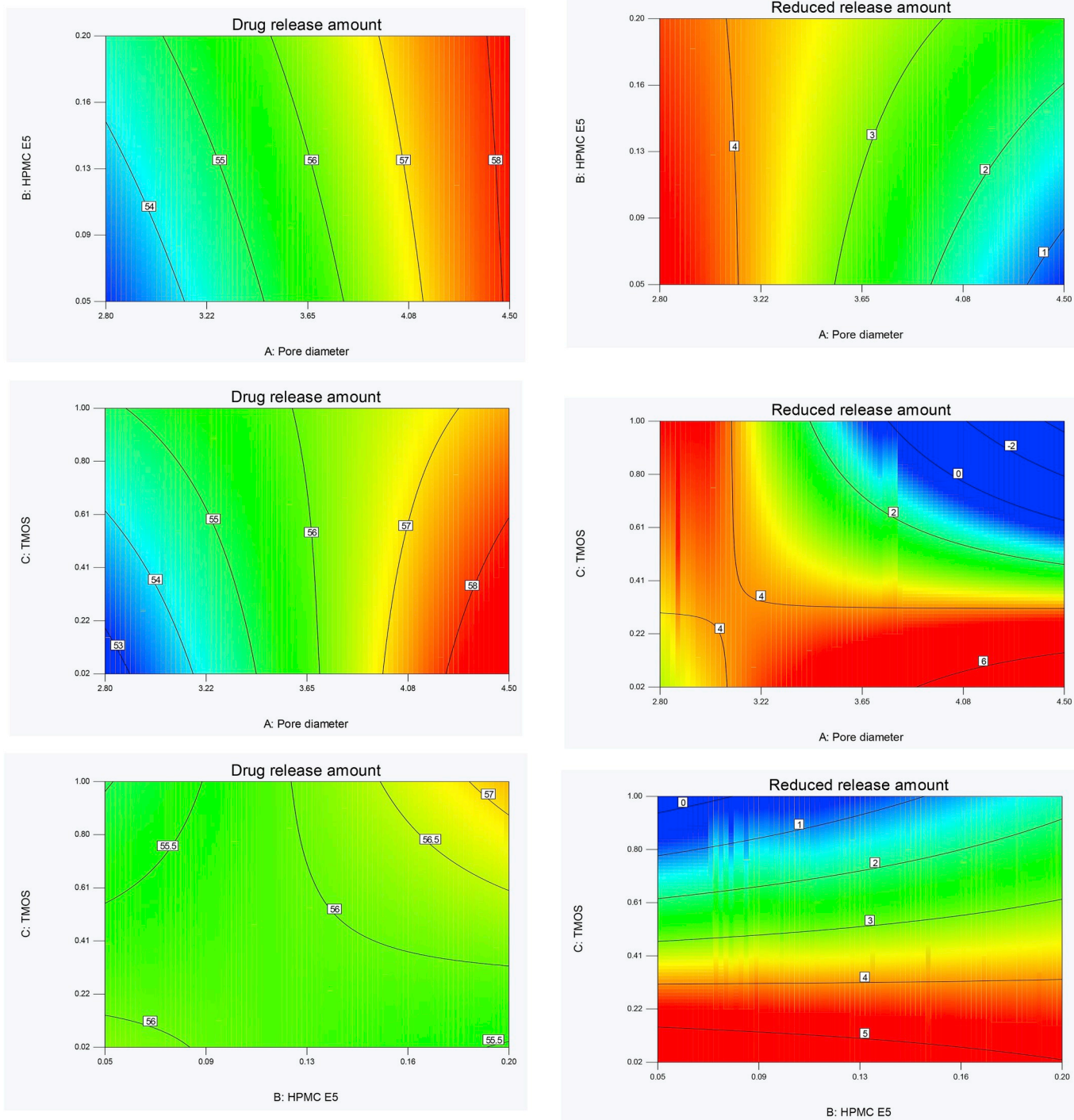


Fig. 6. Contour plots effects of various independent variables on response Y_1 and Y_2 .

amount of HPMC E5 when TMOS amount remained the same in the reaction process, the larger pore diameter carrier had. The reason can be explained that larger micelles were formed by higher amount of HPMC E5 and therefore obtaining silica frame with larger pores. Furthermore, the pore diameter of carrier was not positively related with TMOS used in the synthesized process, giving hint that the silica frame amount had no relationship with pore diameter. Therefore, it was necessary to control TMOS to get desired pore diameter.

3.4.2. Contour plots and response surface analysis

2D contour plots and 3D response surface plots were presented in

Fig. 6 and Fig. 7, and they were favorable to clearly comprehend interaction of factors on the responses. For drug release amount, 2D contour plots of pore diameter with HPMC E5 and pore diameter with TMOS showed that pore diameter was the determined factor among the three parameters. Drug release amount increased with improving the pore diameter of carrier while the effects of HPMC E5 and TMOS on drug release amount were weaker than pore diameter. From 2D contour plots of HPMC E5 with TMOS, it demonstrated again the weak effect of HPMC E5 and TMOS on drug release amount. Furthermore, high drug release amount of more than 56.5% can be achieved when the usage of HPMC E5 was in the range of 0.16–0.2 mL and TMOS was within 0.61–1.0 mL.

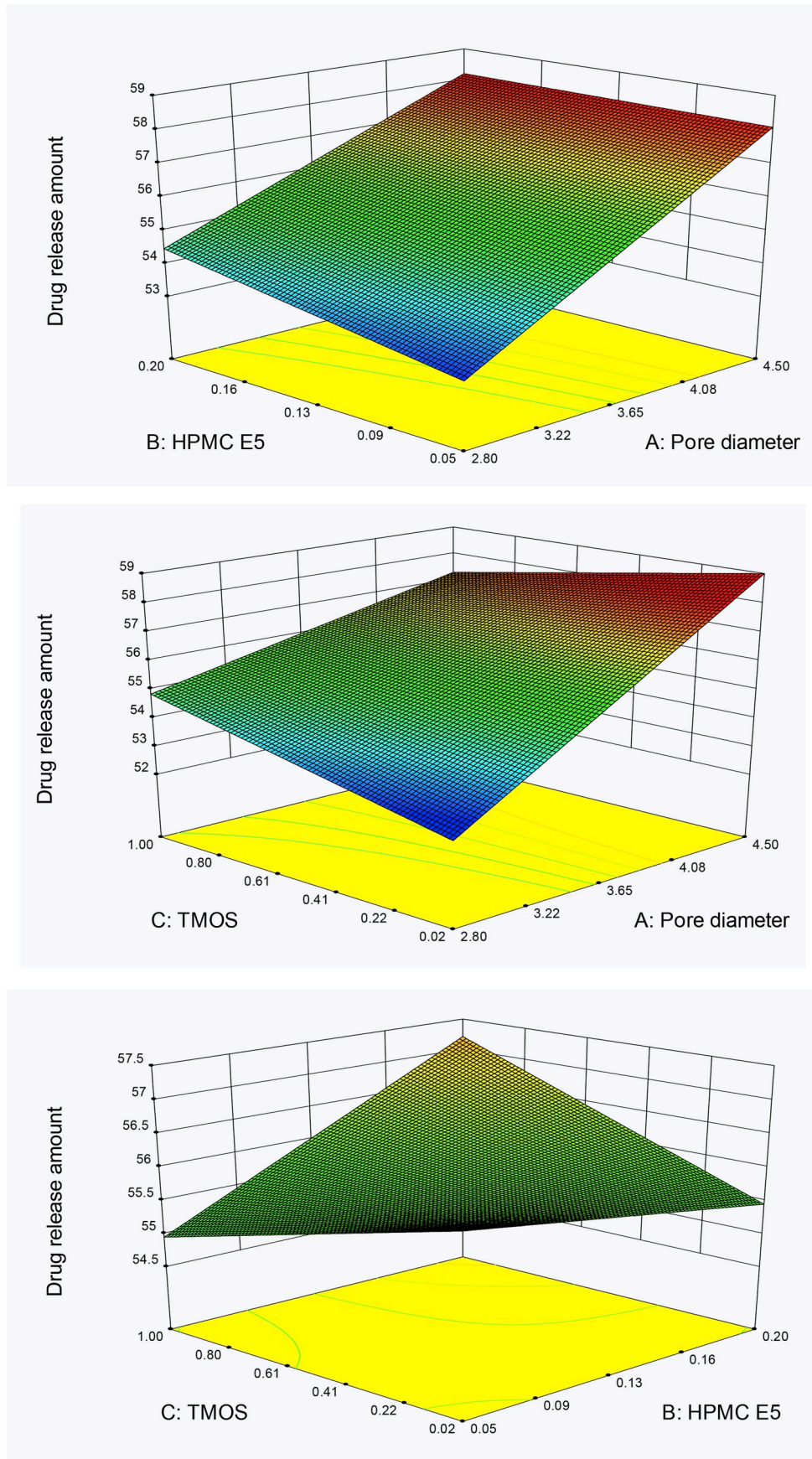
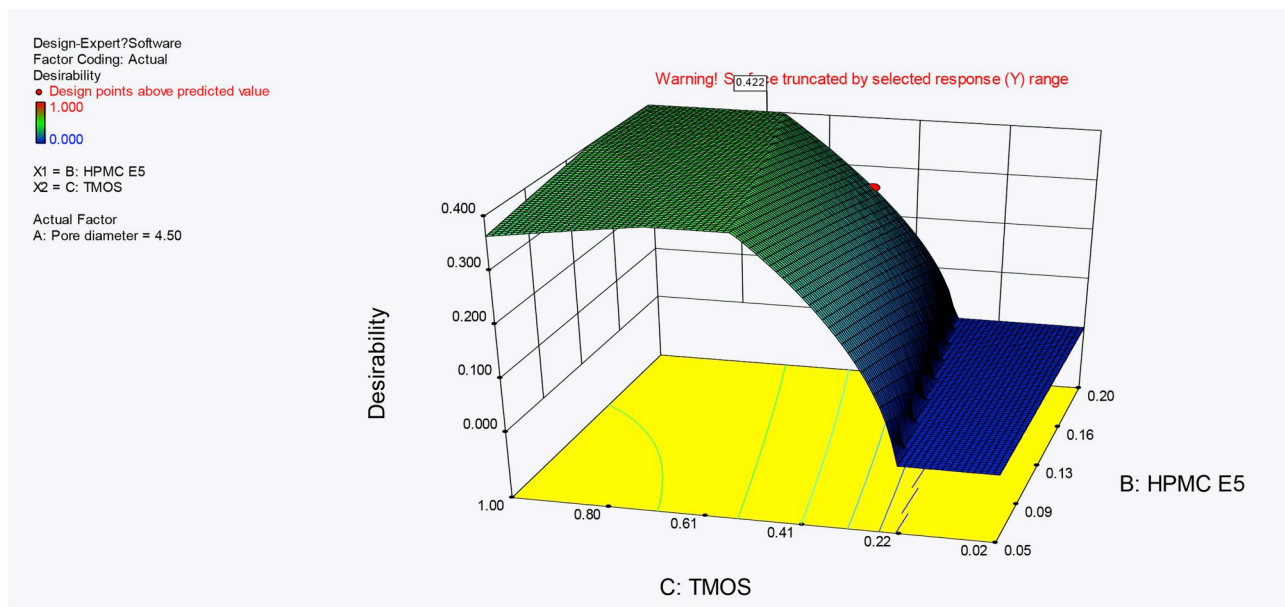
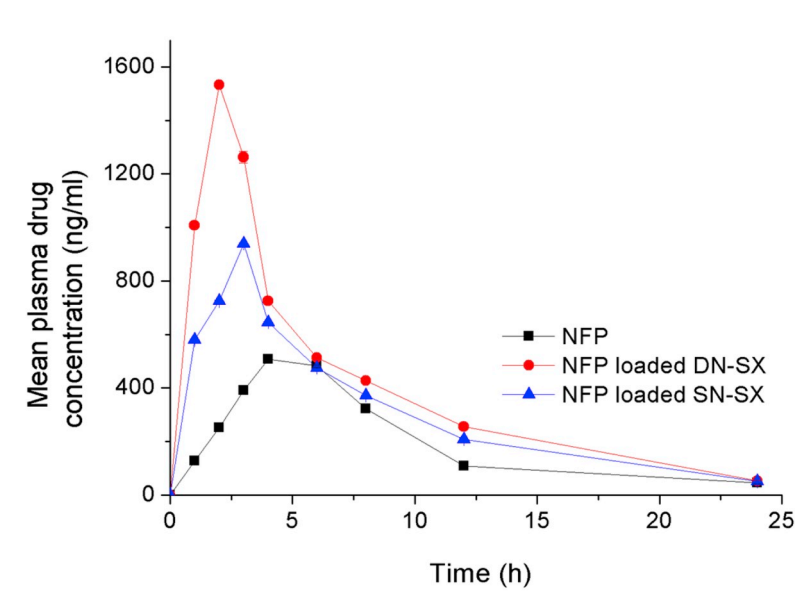


Fig. 7. Response surface plots effects of various independent variables on responseY₁ and Y₂.



A



B

Fig. 8. A, Optimization result of DN-SX as NFP carrier; B, In vivo pharmacokinetic curves of NFP, NFP loaded of DN-SX and NFP loaded SN-SX.

As for reduced drug release amount, 2D contour plots of pore diameter with HPMC E5 showed that low reduced drug release amount can be obtained by using carrier with large pore diameter of more than 4 nm while it had no close relationship with HPMC E5. When attention moved to 2D contour plots of pore diameter with TMOS, it turned out that pore diameter in the range of 3.7–4.5 nm and TMOS within the usage of 0.61–1.0 mL contributed to extreme low reduced drug release amount. Finally for 2D contour plots of HPMC E5 with TMOS, reduced drug release amount had no close connection with HPMC E5 but the consumption of TMOS should reach more than 0.7 mL. Therefore, pore diameter in the range of 3.7–4.5 nm and TMOS within the usage of 0.7–1.0 mL were the favorable working conditions for achieving low reduced drug release amount.

3D response surface plots displayed the whole interactive function of

two parameters on the response. As seen in 3D response surface plots of drug release amount group, the response surface of pore diameter with HPMC E5 and pore diameter with TMOS covered area with almost a flat slope while the response surface of HPMC E5 with TMOS occupied area with obvious curve surface, indicating that the former two interact factors showed direct effect but HPMC E5 with TMOS had relative complicated influence on drug release amount. It further confirmed that pore diameter was the determined factor and large pore diameter was the basic condition for achieving high drug release amount. One important matter can be obtained from 3D response surface plot of pore diameter with TMOS, the usage of TMOS should not be high when applying the carrier with pore diameter of more than 3.7 nm, which possibly because the more silica frame would interfere the residual drug that loaded in the inner pores of carrier. As for 3D response surface plot

Table 3

Optimized DN-SX with the observed and predicted response values for different strengths.

No.		1	2
Pore diameter (nm)		4.50	4.50
HPMC E5 (mL)		0.20	0.74
TMOS (mL)		0.20	0.73
Y ₁	Predicted	58.16	58.14
	Observed	58.20	58.13
Y ₂	Predicted	0.00	0.00
	Observed	0.00	0.00
Desirability		0.422	0.421

Table 4

In vivo pharmacokinetic parameters of NFP, NFP loaded of DN-SX and NFP loaded SN-SX. Student's one-way ANOVA was employed to analyze the obtained parameters. Difference below the probability level of 0.05 (*) was considered as statistically significant and the level lower than 0.001 (**) was extremely significant.

Parameters	NFP	NFP loaded DN-SX	NFP loaded SN-SX
C _{max} (ng/ml)	508.41 ± 4.86	1533.33 ± 4.68**	939.56 ± 4.14**
T _{max} (h)	4 ± 0	2 ± 0	3 ± 0
T _{1/2} (h)	5.72 ± 0.19	5.30 ± 0.15*	5.56 ± 0.06
AUC _{0–24h}	4639.00 ± 34.80	10059.21 ± 46.75**	7475.33 ± 77.25**
AUC _{0–∞}	5017.24 ± 3.78	10462.98 ± 24.85**	7881.44 ± 70.11**
MRT _{0–24h}	7.61 ± 0.06	6.04 ± 0.04*	6.77 ± 0.02*
MRT _{0–∞}	9.47 ± 0.26	7.03 ± 0.11*	8.07 ± 0.05

of HPMC E5 with TMOS, high drug release amount can be received when enhancing one factor with the other factor being the highest point. As seen in 3D response surface plots of reduced drug release amount group, the response surface of pore diameter with HPMC E5 and HPMC E5 with TMOS covered area with almost a flat slope while the response surface of pore diameter with TMOS occupied area with obvious curve surface, indicating that pore diameter with HPMC E5 and HPMC E5 with TMOS exerted direct effect while pore diameter with TMOS performed relative complicated influence on reduced drug release amount. As seen from 3D response surface plots of pore diameter with HPMC E5 and HPMC E5 with TMOS, it was clear that large pore diameter and high usage of TMOS were favorable to get low reduced drug release amount. One crucial point can be obtained from 3D response surface plot of pore diameter with TMOS, low reduced drug release amount can be obtained when increasing one factor with the other factor being the highest point. The above elucidation was valuable instruction for comprehending the relationship between the three parameters with drug release behavior responses.

3.4.3. Optimization

The optimized DN-SX was selected based on the criteria of obtaining highest drug release amount and lowest reduced drug release amount. The two optimized compositions with the highest desirability were chosen and displayed in Fig. 8A and Table 3. It showed that pore diameter and HPMC E5 were the largest in their application range while TMOS can be changeable. The optimization result was in agreement with the conclusions obtained from contour plots and response surface analysis. Pore diameter was the determined factor for the two responses and the larger pore diameter, the better. Since the more micelles formed by HPMC E5 led to larger pore diameter, HPMC E5 should be 2.0 mL. The usage of TMOS was 0.74 mL and 0.73 mL for the two optimizations respectively, which was in the range of 0.7–1.0 mL, showing the optimizations were in accordance with the conclusions drawn from contour plots and response surface analysis. After optimization, the two samples were prepared according to the optimized prescription. The observed response values were quite close to predicted response values, confirming the good predictability and desirability of this three-level two-factorial Box–Behnken experimental design.

3.5. Pharmacokinetic study

After obtaining DN-SX with desired applications, NFP loaded DN-SX was established. Significantly improved dissolution rate for NFP loaded DN-SX and NFP loaded SN-SX led to further assessment of bioavailability to study their in vivo benefit. Mean plasma concentration time profile was depicted in Fig. 8B, while the pharmacokinetic parameters were mentioned in Table 4. For crystalline NFP, the C_{max} was found to be 508.41 ± 4.86 ng/mL, which were 2.02-fold and 0.85-fold significant lower than NFP loaded DN-SX and NFP loaded SN-SX respectively. By using the two carriers, the T_{max} and T_{1/2} turned shorter, demonstrating that the highest drug concentration can be reached at earlier time than NFP since the two carriers successfully converted drug crystalline to amorphous state and finally improved drug dissolution [14,29–32]. For these parameters with statistical analysis, NFP loaded DN-SX was superior to NFP loaded SN-SX, which contributed to both nanoparticles and micelles in the system. After calculating, the relative bioavailability of NFP loaded DN-SX and NFP loaded SN-SX were 216.84% and 161.14% respectively, showing the significant improvement of oral bioavailability by applying the two carriers. It should be noted that the second nano in DN-SX, which was the micelles, exerted crucial functions in achieving highest relative bioavailability among the three samples.

4. Conclusion

The presented paper studied the facile synthesis of DN-SX with double-nano structure and its superiority in delivering NFP. Both DN-SX and SN-SX were quite small nanoparticles aggregated intensively due to xerogel state. DN-SX nanoparticles gathered and shaped like big spherical particles owing to its micelles while SN-SX nanoparticles not. The micelles in DN-SX contributed to obtain large mesopores around 10 nm and resulted in higher surface area and pore volume than SN-SX. NFP was well loaded in the mesopores of the two carriers and drug crystalline state changed from crystalline state to amorphous phase according to DSC analysis. Several major conclusions were made from Box–Behnken experimental design to learn how response reacted as changing each influencing factor. (1) Pore diameter was the determined factor among the three parameters and drug release amount increased with improving the pore diameter of carrier. (2) High drug release amount can be achieved when the usage of HPMC E5 was in the range of 0.16–0.2 mL and TMOS was within 0.61–1.0 mL (3) Pore diameter in the range of 3.7–4.5 nm and TMOS within the usage of 0.7–1.0 mL were the favorable working conditions for achieving low reduced drug release amount. After optimization, HPMC E5 was 2.0 mL and the usage of TMOS was 0.74 mL or 0.73 mL for the two optimizations respectively, showing the optimizations were in agreement with the conclusions drawn from contour plots and response surface analysis. With the DN-SX obtained by optimization, in vivo pharmacokinetic study was conducted and result showed that the relative bioavailability of NFP loaded DN-SX and NFP loaded SN-SX were 216.84% and 161.14%. The optimized DN-SX with double-nano structure provided huge value and application for poorly water soluble drugs.

Declaration of competing interest

The authors declare that they have no known competing financial interests or personal relationships that could have appeared to influence the work reported in this paper.

CRediT authorship contribution statement

Ping Zhang: Conceptualization, Methodology. **Qiankun Jiang:** Formal analysis, Data curation. **Yue Zheng:** Writing - review & editing. **Jing Li:** Writing - original draft.

References

- [1] F.Z. Liang Yan, Jing Wang, Yan Zu, Zhanjun Gu, Yuliang Zhao, *Adv. Mater.* 1805391 (2019) 1–33.
- [2] I. N. Daniel Mihai Teleanu, Valentina Grumezescu, R.I. T. Alexandru Mihai Grumezescu, *Nanomaterials* vol. 9 (2019) 1–18.
- [3] M. Abd Elkodous, Gharieb S. El-Sayyad, Ibrahim Y. Abdelrahman, A.E.M. Hanan, S. El-Bastawisy, Farag M. Mosallam, Hebatallah A. Nasser, A.B. Mohamed Gobara, Mohamed A. Elsayed, Ahmed I. El-Batal, *Colloids Surfaces B Biointerfaces* 180 (2019) 411–428.
- [4] S.S.N. Sangeeta Yadav, V.V.R. Sai, Jitendra Satija, *Food Res. Int.* 119 (2019) 99–109.
- [5] *Adv. Drug Deliv. Rev.* 64 (2012) 37–48.
- [6] S.K. Ji Young Kim, Rodolfo Pinal, Kinam Park, *J. Control. Release* 152 (2011) 13–20.
- [7] U.Y. Yogesh Kadam, Anita Bahadur, *Colloids Surfaces B Biointerfaces* 72 (2009) 141–147.
- [8] Geneviève Gaucher, Prashant Satturwar, Marie-Christine Jones, Alexandra Furto, J.-C.L., *Eur. J. Pharm. Biopharm.* 76 (2010) 147–158.
- [9] *Frontiers in Chemistry* 7 (2019) 1–12.
- [10] D.W. Lijun Sun, Yu Chen, Liying Wang, Ping Huang, Yaping Li, Ziwei Liu, Heliang Yao, Jianlin Shi, *Biomaterials* 133 (2017) 219–228.
- [11] F.L. Xinxin Zhang, Shiyan Guo, Xi Chen, Xiaoli Wang, Juan Li, Yong Gan, *Biomaterials* 35 (2014) 3650–3665.
- [12] J. Li, L. Xu, H. Liu, Y. Wang, Q. Wang, H. Chen, W. Pan, S. Li, *Int. J. Pharm.* 467 (2014) 9–18.
- [13] C.A. McCarthy, R.J. Ahern, R. Dontireddy, K.B. Ryan, A.M. Crean, *Expert Opin. Drug Deliv.* 13 (2016) 93–108.
- [14] J.Z. Yanzhuo Zhang, Tongying Jiang, Siling Wang, *Int. J. Pharm.* 410 (2011) 118–124.
- [15] Y. Wang, Q. Zhao, N. Han, L. Bai, J. Li, J. Liu, E. Che, L. Hu, Q. Zhang, T. Jiang, S. Wang, *Nanomed. Nanotechnol. Biol. Med.* 11 (2015) 313–327.
- [16] E.C. Dengler, J. Liu, A. Kerwin, S. Torres, C.M. Olcott, B.N. Bowman, L. Armijo, K. Gentry, J. Wilkerson, J. Wallace, X. Jiang, E.C. Carnes, C.J. Brinker, E. D. Milligan, *J. Control. Release : official journal of the Controlled Release Society* 168 (2013) 209–224.
- [17] P.N. Durfee, Y.S. Lin, D.R. Dunphy, A.J. Muniz, K.S. Butler, K.R. Humphrey, A. J. Lokke, J.O. Agola, S.S. Chou, I.M. Chen, W. Wharton, J.L. Townson, C. L. Willman, C.J. Brinker, *ACS Nano* 10 (2016) 8325–8345.
- [18] R.L. Na Fan, Pingping Ma, Xin Wang, Li Chang, Li Jing, *Colloids Surfaces B Biointerfaces* 176 (2019) 122–129.
- [19] N. Song, Y.W. Yang, *Chem. Soc. Rev.* 44 (2015) 3474–3504.
- [20] F.Z. Jiahua Zhou, Jing Li, Yongjun Wang, *Mater. Sci. Eng. C* 90 (2018) 314–324.
- [21] J. Li, L. Xu, B. Yang, H. Wang, Z. Bao, W. Pan, S. Li, *Int. J. Pharm.* 492 (2015) 191–198.
- [22] *A.M.a.A.M., Pharmaceutics* 11 (2019) 1–14.
- [23] H.W. Jing Li, Heran Li, Lu Xu, Yingyu Guo, Fangzheng Lu, Weisan Pan, S. Li, *Int. J. Pharm.* 498 (2016) 32–39.
- [29] B. Li, S. Konecke, K. Harich, L. Wegiel, L.S. Taylor, K.J. Edgar, *Carbohydr. Polym.* 92 (2013) 2033–2040.
- [30] T. Vasconcelos, B. Sarmento, P. Costa, *Drug Discov. Today* 12 (2007) 1068–1075.
- [31] C.L.-N. Vo, C. Park, B.-J. Lee, *Eur. J. Pharm. Biopharm.* 85 (2013) 799–813.
- [32] J. Li, L. Xu, H. Wang, B. Yang, H. Liu, W. Pan, S. Li, *Mater. Sci. Eng. C* 59 (2016) 710–716.